

Rafael Kenji Nishihora, Ellen Rudolph, Mara Gabriela Novy Quadri, Dachamir Hotza, Kurosch Rezwan, Michaela Wilhelm



Asymmetric mullite membranes manufactured by phase-inversion tape casting from polymethylsiloxane and aluminum diacetate

Journal Article as: peer-reviewed accepted version (Postprint)

DOI of this document\* (secondary publication): 10.26092/elib/2615

Publication date of this document: 25/10/2023

\* for better findability or for reliable citation

#### Recommended Citation (primary publication/Version of Record) incl. DOI:

Rafael Kenji Nishihora, Ellen Rudolph, Mara Gabriela Novy Quadri, Dachamir Hotza, Kurosch Rezwan, Michaela Wilhelm,  
Asymmetric mullite membranes manufactured by phase-inversion tape casting from polymethylsiloxane and aluminum diacetate,  
Journal of Membrane Science, Volume 581, 2019, Pages 421-429, ISSN 0376-7388,  
<https://doi.org/10.1016/j.memsci.2019.03.047>

Please note that the version of this document may differ from the final published version (Version of Record/primary publication) in terms of copy-editing, pagination, publication date and DOI. Please cite the version that you actually used. Before citing, you are also advised to check the publisher's website for any subsequent corrections or retractions (see also <https://retractionwatch.com/>).

This document is made available under a Creative Commons licence.

The license information is available online: <https://creativecommons.org/licenses/by-nc-nd/4.0/>

#### Take down policy

If you believe that this document or any material on this site infringes copyright, please contact [publizieren@suub.uni-bremen.de](mailto:publizieren@suub.uni-bremen.de) with full details and we will remove access to the material.

---

# Asymmetric mullite membranes manufactured by phase-inversion tape casting from polymethylsiloxane and aluminum diacetate

Rafael Kenji Nishihora<sup>a,b</sup>, Ellen Rudolph<sup>a,c</sup>, Mara Gabriela Novy Quadri<sup>b</sup>, Dachamir Hotza<sup>b</sup>, Kurosch Rezwan<sup>a,d</sup>, Michaela Wilhelm<sup>a,\*</sup>

<sup>a</sup> Institute of Advanced Ceramics, University of Bremen, Am Biologischen Garten 2, IW3, D-28359, Bremen, Germany

<sup>b</sup> Department of Chemical Engineering and Food Engineering (EQA), Federal University of Santa Catarina (UFSC), 88040-900, Florianópolis, SC, Brazil

<sup>c</sup> Department of Mechanical Engineering (EMC), Federal University of Santa Catarina (UFSC), 88040-900, Florianópolis, SC, Brazil

<sup>d</sup> MAPEX Center for Materials and Processes, University of Bremen, 28359, Bremen, Germany

---

## ARTICLE INFO

### Keywords:

Polysiloxane

Mullite

Ceramic membrane

Tape casting

Phase inversion

## ABSTRACT

Polymethylsiloxane (MK) and aluminum diacetate have been stoichiometrically combined to synthesize a mullite-based powder ( $3\text{Al}_2\text{O}_3 \cdot 2\text{SiO}_2$ ) at 850 °C (5 h) or 1200 °C (3 h). High-purity crystalline mullite (> 99%) was obtained by heating the mixture in the air (thermal oxidation) at 1200 °C for 3 h, mainly due to the formation of highly reactive silica and alumina precursors. Afterward, the mullite-based powders were used to prepare planar asymmetric microfiltration membranes by phase-inversion tape casting. The green membranes were sintered at 1600, 1650 or 1700 °C during 2 h. The asymmetric morphology identified in the membranes by scanning electron microscopy analysis reveals a thin skin-layer (microfiltration layer, < 10 μm) followed by a porous support, in which two different structures were observed: finger- and/or sponge-like layer. Water permeation performance in a dead-end configuration was investigated at different pressures (3, 4, and 5 bar). The obtained results clearly indicated an improved water permeation flux compared to a symmetric commercial membrane (133.6 m<sup>3</sup>/m<sup>2</sup>·h compared to 14.7 m<sup>3</sup>/m<sup>2</sup>·h, respectively, at 5 bar). This observation could be ascribed to the asymmetric morphology resultant from the phase-inversion process.

---

## 1. Introduction

A rising interest in ceramic membranes has been observed by the industry and research fields. The development of advanced processing techniques made possible the preparation of high-performance ceramic membranes. In comparison to traditional polymeric membranes, ceramic presents higher chemical and thermal stability, structural resistance, and long working life [1,2]. There are plenty of techniques to prepare ceramic membranes, such as structural leaching, extrusion, pressing, chemical vapor deposition, sol-gel, slip casting, and tape casting [3]. Recently, an increasing number of works have reported the use of phase-inversion (pore forming strategy) coupled with tape casting (shaping method) for the preparation of asymmetric flat ceramic membranes [4–10].

Phase-inversion has been widely used to produce polymeric membranes [11]. However, this process has been adapted to prepare ceramic membranes by simply adding ceramic particles into the polymeric solution and later burning out the organic components and consolidating the structure through sintering [4,12–14]. This method is based on

thermodynamic and kinetic principles, such as the relationship between the chemical potentials and diffusivities of the individual components and Gibb's free energy of mixing of the entire system [15]. The most common phase-inversion strategy is the non-solvent induced process. In this approach, the polymer is converted from the liquid phase into a solid by the phase separation or “demixing” what is induced by a non-solvent (normally water) [16]. The membrane formation is dictated by many parameters, such as slurry composition, particle size, rheological properties, and non-solvent characteristics [13,17]. The main advantage of this technique relies on the flexibility to tailor the morphology in order to produce an asymmetric structure composed by a thick sub-layer (porous support) and a thin layer (membrane). Therefore, this one-step approach is possible by adjusting one of the aforementioned parameters, which can result in different morphologies in the sub-layer (e.g. finger or sponge-like structures) [18].

The predominant materials used to prepare ceramic membranes include α-alumina, silica, zirconia, titania, perovskites, and aluminum silicates (e.g. mullite). Mullite is the only stable crystalline phase in the alumina-silica ( $\text{Al}_2\text{O}_3\text{-SiO}_2$ ) system under normal atmospheric pressure

---

\* Corresponding author.

E-mail address: [mwilhelm@uni-bremen.de](mailto:mwilhelm@uni-bremen.de) (M. Wilhelm).

and its composition varies in the range of  $3\text{Al}_2\text{O}_3\cdot 2\text{SiO}_2$  to  $2\text{Al}_2\text{O}_3\cdot \text{SiO}_2$  [19]. This material presents a great importance in both traditional and advanced ceramics, which is directly related to its particular properties: high thermal stability, low thermal expansion, high resistance to creep, corrosion stability, low density (compared to pure  $\alpha$ -alumina), good mechanical strength and fracture toughness [20,21]. The traditional method to produce mullite requires high temperature ( $> 1587^\circ\text{C}$ ) and holding times. Exploring reactive silica and/or alumina precursors has been one strategy to produce pure mullite under mild conditions. For instance, highly reactive amorphous silica has been prepared by thermal-oxidation of polysiloxanes [22]. Even though high-purity mullite ( $> 99\%$ ) has been produced by combining polysiloxanes and microsized ( $0.8\ \mu\text{m}$ )  $\alpha$ - $\text{Al}_2\text{O}_3$  [22] and nanosized ( $15\ \text{nm}$ )  $\gamma$ - $\text{Al}_2\text{O}_3$  [23], the temperatures applied were in the range of  $1700^\circ\text{C}$  and  $1350^\circ\text{C}$ , respectively. Alternatively, recent studies have reported the preparation of mullite membranes using materials like natural bauxite [24] with fly ash [25,26], and kaolin-based powders [27]. In particular, kaolin can form mullite at temperatures up to  $1200^\circ\text{C}$  [28]. However, the resultant mullite phase is accompanied by cristobalite ( $\text{SiO}_2$ ) [27]. Hence, some works include extra alumina content and a crystallization catalyst (e.g.  $\text{AlF}_3$ ) to enhance mullitization, yet impurities such as corundum and cristobalite phases are still commonly found [29,30].

With the purpose of exploring an alternative alumina source to prepare high-purity mullite powder in conjunction with silica originated from a polysiloxane, the present work reports the use of aluminum diacetate [31] and polymethylsiloxane. The prepared mullite-based powder was characterized with regard to particle size distribution and crystallinity. Afterward, phase-inversion tape casting was employed to prepare planar asymmetric microfiltration mullite membranes using the synthesized powder. The sintering temperature was varied and the prepared membranes were evaluated in terms of morphology, crystallinity, macroporosity, mechanical strength, and water permeation flux.

## 2. Experimental

### 2.1. Materials

A commercially available methyl-polysiloxane (PMS Silres MK<sup>®</sup>, Wacker) was used as the starting preceramic polymer and silica source. Aluminum diacetate ( $\text{C}_4\text{H}_7\text{AlO}_5$ , purum p.a., Sigma-Aldrich) was used as alumina source. For comparison purposes,  $\alpha$ -alumina (Almatis, CT3000,  $d_{50} \sim 0.5\ \mu\text{m}$ ) was also used as alumina source for the preparation of mullite. For the production of the asymmetric membranes, a polyethersulfone (PES, 58,000 g/mol, GoodFellow Cambridge Limited) was selected as the polymer source and polyvinylpyrrolidone (PVP – K40, Sigma-Aldrich) as an additive. The solvent for the polymer and liquid medium for the ceramic particles was *N*-methyl-2-pyrrolidone (NMP, Sigma-Aldrich).

### 2.2. Mullite-based powder preparation

The MK powder was dissolved in acetone (1 g of MK per 50 mL of acetone) [23] and stirred for 15 min. Then the alumina or aluminum diacetate [31] was added based on a stoichiometric proportion to produce pure mullite phase ( $3\text{Al}_2\text{O}_3\cdot 2\text{SiO}_2$ ). The mixture was ultrasonicated for 10 min and stirred in a closed beaker during 3 h and further 4 h with the beaker open. To ensure further solvent removal and pre-crosslink of the polysiloxane, an additional thermal treatment step was employed for 12 h at  $70^\circ\text{C}$ . In order to get a fine powder, the obtained solid material was ground in a ball mill for 6 h at 350 rpm. Afterward, the fine powder was calcined at  $850^\circ\text{C}$  (5 h) or  $1200^\circ\text{C}$  (3 h) with a heating/cooling rate of  $5^\circ\text{C}/\text{min}$  [31]. The final powder was characterized and applied to produce the ceramic membranes. The preparation steps of the mullite-based powder are shown in Fig. 1a.

### 2.3. Membrane preparation

The slurries compositions are given in Table 1. The polyethersulfone and polyvinylpyrrolidone were dissolved in *N*-methyl-2-pyrrolidone. After the polymer solution was formed, the mullite-based powder was added and stirred for 24 h at room temperature. The as-prepared slurry was degassed for 30 min using a vacuum pump (20 mbar). Then, the slurry was cast over a polyethylene terephthalate carrier film (Mylar, G10JRM, Richard E. Mistler, Inc.) with a doctor blade using a gap height of 1.2 mm. The cast slurry was solidified by immersion precipitation in deionized water (non-solvent) for 24 h at room temperature. Afterward, the green tape was dried in the fume hood at room temperature for 3 days. The dried green tape was cut into desired shape and size, heated at a rate of  $3^\circ\text{C}/\text{min}$  to  $850^\circ\text{C}$  in air, and kept at that temperature for 3 h to remove the organic moieties. Then the samples were heated at a rate of  $2^\circ\text{C}/\text{min}$  to final temperature ( $1600$ – $1650$ – $1700^\circ\text{C}$ ) and kept at that temperature for 2 h in air, and cooled down at a rate of  $2^\circ\text{C}/\text{min}$  to room temperature. The preparation steps of the membranes are illustrated in Fig. 1b.

### 2.4. Specimen denotation

The mullite-based powders were prepared with MK (silica source) and either  $\alpha$ -alumina or aluminum diacetate as alumina source. The ceramic powder denotation is given by the alumina source accompanied by the calcination temperature. For instance, Diac-850 means that the aluminum diacetate is the alumina source plus MK calcined at  $850^\circ\text{C}$ , and Alu-850 means that the aluminum diacetate is the alumina source plus MK calcined at  $850^\circ\text{C}$ . In addition, in the case of membranes denotation, the sintering temperature is added as follows: Diac-850-1700 indicates the mullite-based powder used (as aforementioned) followed by the sintering temperature of the membrane produced ( $1700^\circ\text{C}$ ).

### 2.5. Characterization

The macrostructure of the powder and membranes was analyzed by Scanning Electron Microscopy (SEM, 20 kV; Series 2, Obducat CamScan; Supra 40-Carl Zeiss). For this purpose, the samples were sputtered with gold (K550, Emitech, Judges Scientific). In order to evaluate the skin-layer thickness and the pore sizes presented on the bottom and top surface of the sintered membranes, the SEM images were processed and analyzed by an image processing software (ImageJ) [32]. The number of pores detected from the SEM images varied from around 400 up to 1200 data points accounted. The particle size distribution of the mullite-based powder was measured by a laser diffraction device (Malvern Mastersizer 2000). The density of these powders was acquired by Helium Pycnometer (Pycnometer, Porotec). Porosity and pore size distributions of the tapes were determined using mercury intrusion porosimetry (Pascal 140/440, Porotec). X-ray diffraction analysis (powder XRD, Seifert 3003) was conducted to identify the obtained crystal phases from both calcined powders and sintered membranes. In order to quantify the composition in terms of crystal phases, Rietveld refinement was performed with the diffractograms by a software (MAUD – Material Analysis Using Diffraction, version 2.84, December 7, 2018) [33]. The MAUD software was developed to analyze diffraction spectra and determine crystal structures, quantify the relative contribution of crystalline phases, and microstructure of phases along with the texture and residual stresses. A detailed documentation about the software usage is available online [34]. The reference diffractograms can be obtained from the Crystallography Open Database (COD), which is an open-access collection of crystal structures of organic, inorganic, metal-organic compounds and minerals (excluding biopolymers) [35,36].

The mechanical behavior of the sintered tapes was studied by three-point bending tests (Roell Z005, Zwick – [37]). These measurements

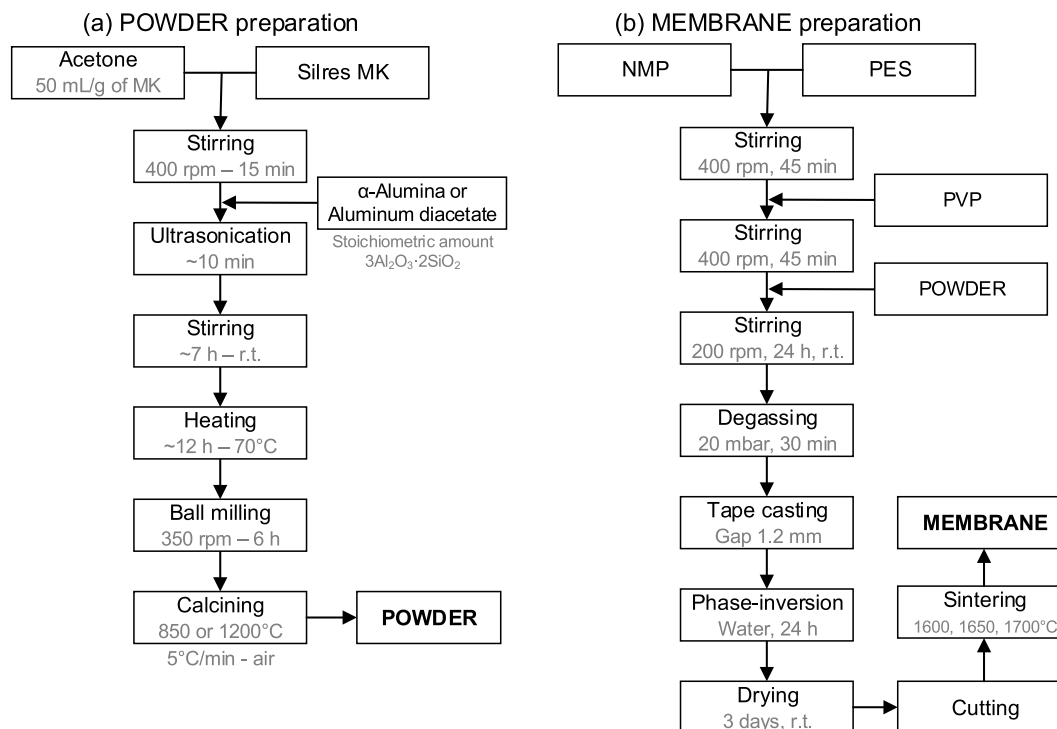


Fig. 1. Process scheme of the preparation of mullite-based (a) powder and (b) membrane.

Table 1

Slurry compositions (vol%) for the preparation of the mullite-based membranes.

Material	Slurry 1, 2 (vol%)	Slurry 3 (vol%)
N-methyl-2-pyrrolidone (NMP)	67.14	65.21
Polyethersulfone (PES)	6.22	8.15
Polyvinylpyrrolidone (PVP-40)	0.79	0.79
Ceramic powder (mullite-based powders)	25.85	25.85

Slurry 1, 2: Ceramic powder – Diac-850 (2.591 g/cm<sup>3</sup>) or Diac-1200 (3.045 g/cm<sup>3</sup>).

Slurry 3: Ceramic powder – Alu-850 (3.134 g/cm<sup>3</sup>). Note: in order to improve the processability of the Slurry 3 and produce a homogenous and stable green membrane, the PES amount was increased accompanied by the decreasing of NMP content.

Density of the ceramic powders was measured using Helium Pycnometer device (Pycnomatic, Porotec).

were performed using a 5 kN load cell (piezoelectric force sensor). The samples were cut into a rectangular shape (16 mm length, ~2 mm width, and 0.7–1.0 mm thickness) and placed in the center of a sample holder with 10 mm distance between the support rollers (diameter of 1.5 mm). The crosshead speed and pre-load were fixed at 0.1 mm min<sup>-1</sup> and 0.25 N, respectively. Twenty samples for each composition and temperature were tested and statistically evaluated by Weibull analysis. Water permeation tests were performed using a homemade setup in a dead-end configuration (see Fig S. 1). The membranes were cut into a circular shape (10 mm diameter) and tested in triplicate at various pressures. For comparison, a commercially available borosilicate glass membrane (Por5, Robugas) was also tested. The permeation flux was calculated according to the following equation:

$$J = \frac{1}{A} \cdot \frac{dV}{dt} \quad (1)$$

where  $J$  is the membrane permeation flux (m<sup>3</sup>·m<sup>-2</sup>·h<sup>-1</sup>);  $A$  is the effective transverse area of the ceramic membrane (m<sup>2</sup>);  $dV$  and  $dt$  represent the variation in volume (m<sup>3</sup>) and time (h), respectively.

### 3. Results

Preparation of mullite-based powder was performed by using a commercially available polysiloxane (MK) as silica precursor, and either commercially available  $\alpha$ -alumina powder or aluminum diacetate as alumina sources. From the prepared mullite-based powders, micro-filtration ceramic membranes were successfully produced by phase-inversion tape casting method. The green bodies were stable and easy to handle. The produced tapes presented an average thickness of ~1.0 mm and a cut area of 10 × 20 cm, as obtained prior to sintering. The samples for the mechanical test were cut into rectangular shapes (5 × 3 cm), whose dimensions were adjusted after sintering to the required specifications for the test. The samples for permeation tests were cut into circles (diameter: 2.5 cm) and/or squares (2.5 × 2.5 cm). It is noteworthy that the warping during sintering constitutes one of the major technological challenges to produce large sizes of ceramic membrane plates. However, there are some strategies frequently used even in industrial scales such as applying the vertical or overhanging sintering [38], supported and vertically inclined sintering, and over-stacking samples or using ceramic weights (e.g. inert inorganic powder, ceramic pieces, etc) [39]. The particle size and sintering temperature were varied to investigate their influence on pore structure, mechanical properties, and water permeation flux.

#### 3.1. Powder size and composition

Fig. 2 shows SEM images (left) of the prepared powders alongside with the particle size distributions measured by laser diffraction (right). The SEM images evidence the tendency to form agglomerates, especially due to increases in temperature and by using  $\alpha$ -alumina as alumina source. The particle size distribution analysis corroborates the SEM findings by exhibiting narrower size distribution for Diac-850 sample (mean particle size of 5.3  $\mu$ m), which is slightly enlarged by increasing the calcination temperature up to 1200 °C (Diac-1200, mean particle size: 6.4  $\mu$ m). However, the substitution of aluminum diacetate by  $\alpha$ -alumina has a great impact on particle size, even at the lower calcination temperature (850 °C). As a result, the specimen Alu-850

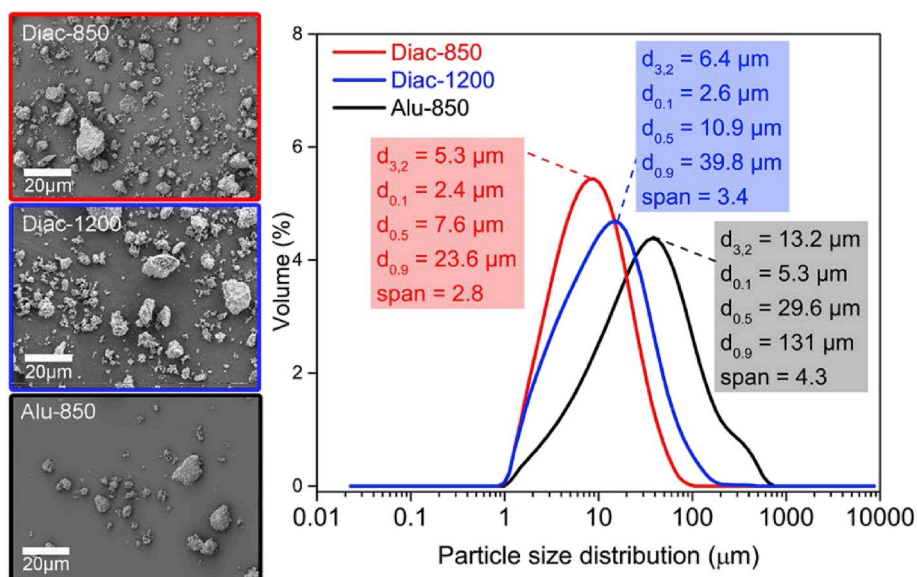


Fig. 2. SEM images (left) of the prepared mullite-based powders and particle size distribution analysis by laser diffraction (right).

shows the widest range of particle size distribution (span = 4.3), where the mean value was further raised up to 13.2  $\mu\text{m}$ . Since the sample Alu-1200 resulted in a single agglomerated block after calcination, this composition was not suitable to be measured and, hence impracticable to prepare stable microfiltration membranes. Therefore, the membranes were prepared using the Diac-850, Diac-1200, and Alu-850 powders.

The investigation of the mullitization process of the calcined powders is shown in Fig. 3. The Alu-850 specimen does not exhibit any peak characteristic of mullite, expressing only the  $\alpha$ -alumina phase. The same is true for the Alu-1200, shown here for comparison purposes since it was not studied for membrane preparation as justified before. The Diac-850 is completely composed by amorphous phase at this temperature, which explains the lower density value obtained for this powder (2.591  $\text{g}/\text{cm}^3$ ) in comparison to the literature value for mullite ( $\sim 3.2 \text{ g}/\text{cm}^3$ ) [20]. On the other hand, the Diac-1200 sample features mainly mullite peaks that corroborate with the higher density observed (3.045  $\text{g}/\text{cm}^3$ ). This observation is confirmed by the Rietveld

refinement analysis in which 99.14% of the crystalline phase is composed by mullite (COD ID 2310785). As expected, the mullitization is facilitated by bringing together two reactive precursors, MK and aluminum diacetate. Nonetheless, considering that the Rietveld refinement is only capable of quantifying crystalline portions of the samples, the assumption of the presence of some amorphous contribution may not be excluded at this temperature.

### 3.2. Membrane composition

As presumed, since the lower sintering temperature is above the minimum mullitization temperature, all sintered membranes disclose peaks characteristic of mullite crystalline phase, as shown in Fig. S. 2. Although relatively short holding time has been employed (2 h), the analyzed crystalline phase contains a high degree of mullite given the reactive nature of the amorphous silica formed due the thermooxidation of MK. Table 2 summarizes the crystalline phases content for all sintered membranes using the Rietveld refinement method. There is no perceptible difference among the produced samples, in which mullite content is above 99 wt%. The goodness of fit values are in general in an acceptable range ( $\text{sig} \leq 2$  and  $R_{\text{wp}} \leq 20\%$ ). Notwithstanding corundum represents the most noticeable impurity in the mullite system, its value

Table 2

Crystalline phases content (wt.%) and goodness of fit determined by Rietveld refinement method of the X-ray powder diffractograms from the sintered membranes.

Sample	Crystalline phases content (wt.%)			Goodness of fit	
	Mullite	Corundum	Cristobalite	sig	$R_{\text{wp}}$ (%)
Alu-850-1600	99.96	0.02	0.02	1.85	17.13
Alu-850-1650	99.94	0.00	0.06	2.06	18.61
Alu-850-1700	99.39	0.60	0.01	1.73	17.03
Diac-850-1600	99.97	0.03	0.00	1.86	16.56
Diac-850-1650	99.86	0.00	0.14	2.02	16.86
Diac-850-1700	99.97	0.00	0.03	1.93	16.03
Diac-1200-1600	99.96	0.31	0.00	1.84	17.15
Diac-1200-1650	99.69	0.30	0.01	2.17	18.95
Diac-1200-1700	99.77	0.23	0.00	1.92	16.12

Mullite-COD ID 2310785; Corundum-COD ID 2300448; Cristobalite-COD ID 9001579.

$R_{\text{wp}}$  = weighted profile R-factor.

sig =  $R_{\text{wp}}/R_{\text{expected}}$ .

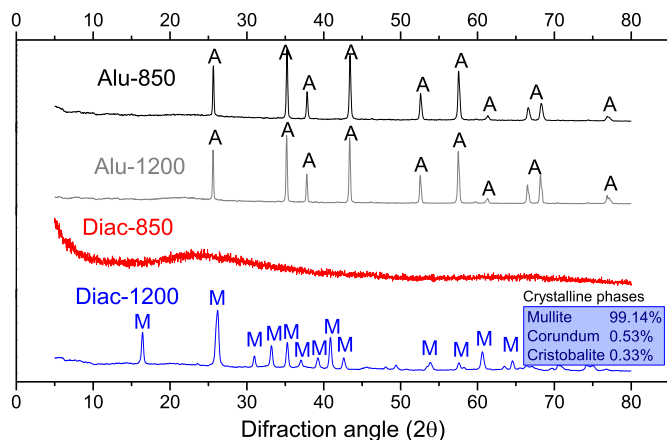


Fig. 3. X-ray diffraction (XRD) analysis of the obtained mullite-based powders. A -  $\alpha$ -Alumina or Corundum (ref.: PDF#04-071-1123); M - Mullite ( $3\text{Al}_2\text{O}_3 \cdot 2\text{SiO}_2$ ) (ref.: PDF#01-079-1454). (The values in the blue box represent the crystalline phases of Diac-1200 sample quantified by Rietveld Refinement; Goodness of fit: sig = 1.5; Rwp = 13.96%; Mullite-COD ID 2310785; Corundum-COD ID 2300448; Cristobalite-COD ID 9001579.). (For interpretation of the references to color in this figure legend, the reader is referred to the Web version of this article.)

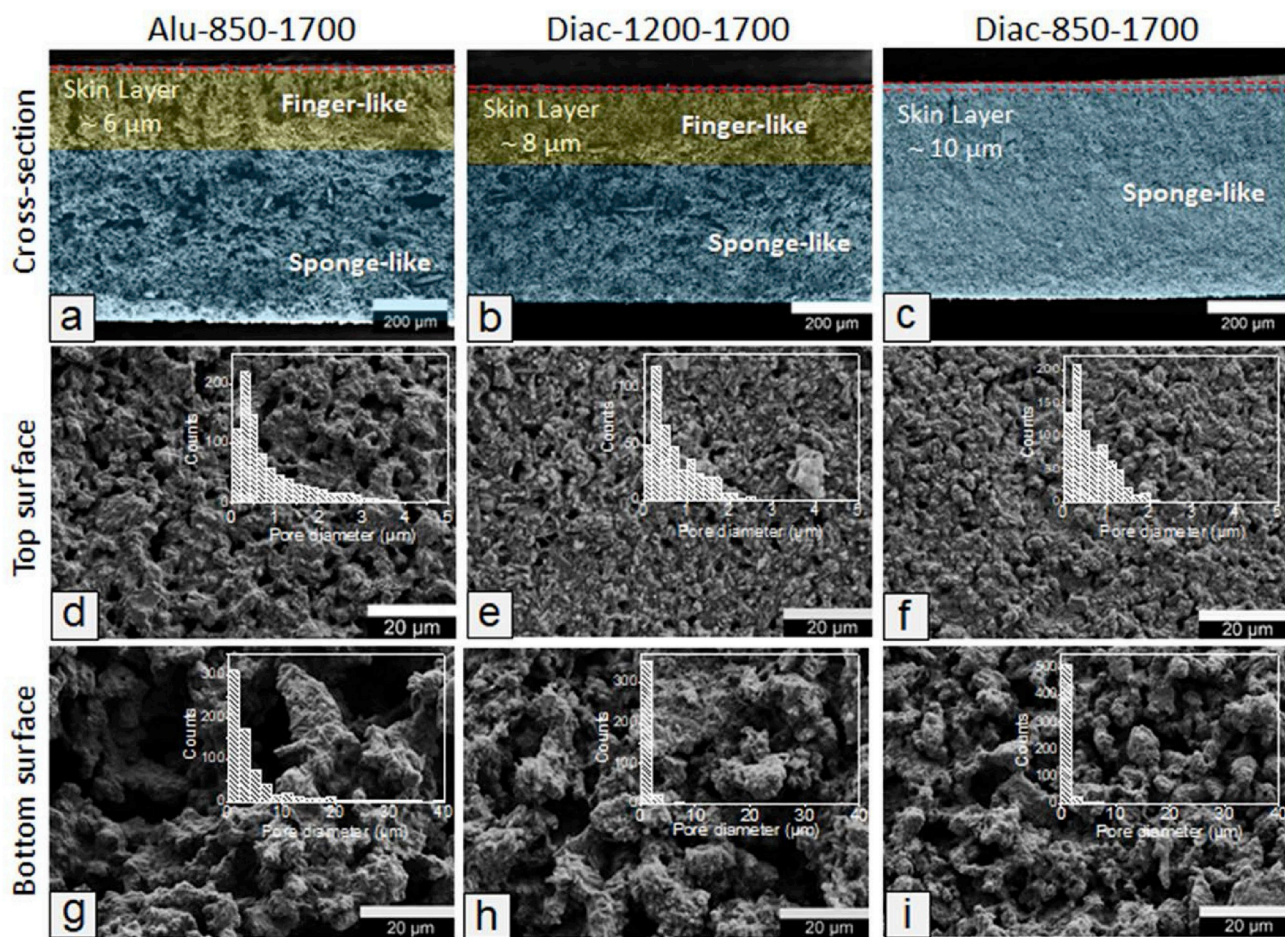


Fig. 4. SEM images of the cross-sections (a, b, c), top surface (d, e, f), and bottom surface (g, h, i) of the membranes sintered at 1700 °C. Pore diameter distribution graphs are displayed for the top and bottom surface based on image analysis using ImageJ.

is not significant in the total crystalline phase ( $< 0.6$  wt%). Even though the Rietveld method is insensitive to amorphous phases (as stated before), given the applied sintering temperatures (above the eutectic temperature,  $\sim 1590$  °C), amorphous contributions are not expected in this case [40,41].

### 3.3. Membrane morphology and macroporosity

Fig. 4a-b-c show the cross-section of the sintered mullite-based membranes (1700 °C) along the thickness direction. These images reveal an asymmetric structure for all the analyzed samples. The upper part is composed by a thin layer (skin layer), in which the thickness varies inversely proportional to the mullite based powder size  $\sim 6$   $\mu\text{m}$  (Alu-850-1700),  $\sim 8$   $\mu\text{m}$  (Diac-1200-1700), and  $\sim 10$   $\mu\text{m}$  (Diac-850-1700). Below the skin layer it is possible to identify a more pronounced porous structure for the samples Alu-850-1700 and Diac-1200-1700. They present the typical finger-like pores (yellow highlighted zone) that were initiated from the top surface of the membrane and penetrated into less than half of the bulk structure. The blue highlighted zone is composed by sponge-like structures, which extends until the bottom surface. Contrastingly, the specimen Diac-850-1700 does not display a three-layered configuration as the other two compositions. Instead, it only exhibits the skin layer followed by a sponge-like structure with a denser aspect.

The top and bottom surface morphologies supplemented by the pore diameter range are shown in Fig. 4d-e-f and Fig. 4g-h-i, respectively. In respect of surface morphology, there is no apparent difference in pore shape, being the main distinction with regard to pore diameter size. The pore diameter range increases according to the ceramic particle size, as

to be expected. Alu-850-1700 presents the wider pore size distribution for both top (Fig. 4d, pore diameter  $< 4$   $\mu\text{m}$ ) and bottom (Fig. 4g, pore diameter  $< 20$   $\mu\text{m}$ ) surface among the displayed samples. Hence, Diac-850-1700 is positioned in the smaller pore diameter range since it was produced using the smaller mullite-based powder. The pore sizes on the top surface are inferior to  $2$   $\mu\text{m}$  (Fig. 4f), while the bottom surface presents values smaller than  $4$   $\mu\text{m}$  with a consistent peak in the  $2$   $\mu\text{m}$  region (Fig. 4i). The intermediate sample, Diac-1200-1700, exhibits values closely related to the sample Diac-850-1700 rather than Alu-850-1700. This response is quite predictable, reflecting the ceramic powder size of the studied samples.

Taking into account the limitation of the image analysis as an exploratory method for determining the pore size, the use of another technique in conjunction is highly advisable. The mercury intrusion analysis is a well-established method for determining pore size distribution and open porosity. Fig. 5a-b-c shows the results of the Hg-intrusion porosimetry of the prepared membranes sintered at different temperatures (1600 °C, 1650 °C and 1700 °C). The detected macropore sizes displayed a quite wide pore size distribution for the samples Diac-1200 (1–10  $\mu\text{m}$ ) and Alu-850 ( $\sim 2$ –20  $\mu\text{m}$ ), for all the sintering temperatures. On the other hand, the samples prepared with Diac-850 exhibit a very narrow distribution in the range of  $1$   $\mu\text{m}$ , especially at 1600 °C and 1650 °C. Regarding the effect of sintering temperature on the pore size distribution, it is basically negligible. Notwithstanding, the open porosity is highly affected by increasing the temperature from 1650 °C to 1700 °C, in which densification is favored. For instance, Diac-1200-1650 decreases from 68.27% to 53.68% at 1700 °C (Diac-1200-1700); Alu-850-1650 from 66.68% to 51.28% at 1700 °C (Alu-

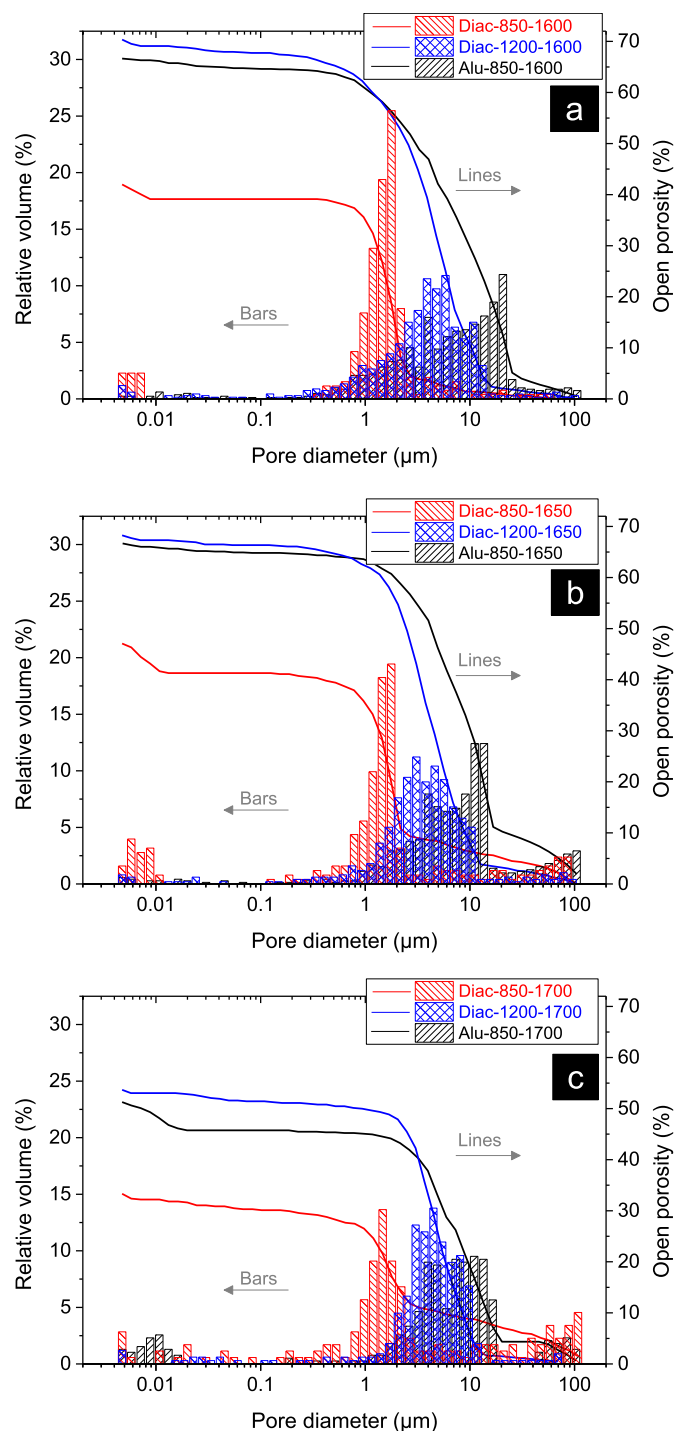


Fig. 5. Pore size distribution ( $\mu\text{m}$ ) versus relative pore volume (%) and open porosity (%) curves obtained from Hg-intrusion porosimetry of the sintered mullite membranes at different temperatures: (a) 1600 °C, (b) 1650 °C and (c) 1700 °C.

850-1700); and Diac-850-1650 reduces from 47.08% to 33.33% at 1700 °C (Diac-850-1700). In terms of percentage reduction, all the samples show a similar range of open porosity diminution (14–15%)

### 3.4. Mechanical behavior of sintered membranes

Fig. 6a shows the Weibull failure distribution of the flexural strength of selected sintered membranes, exhibiting their respective characteristic flexural strength ( $\sigma_0$ ) and Weibull modulus ( $m$ ). The Alu-

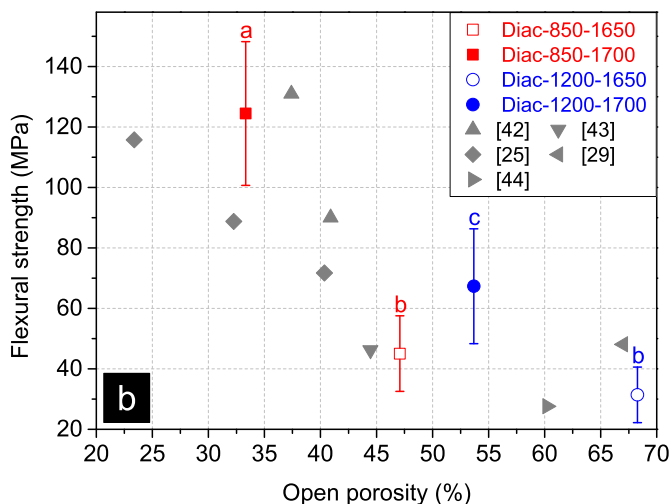
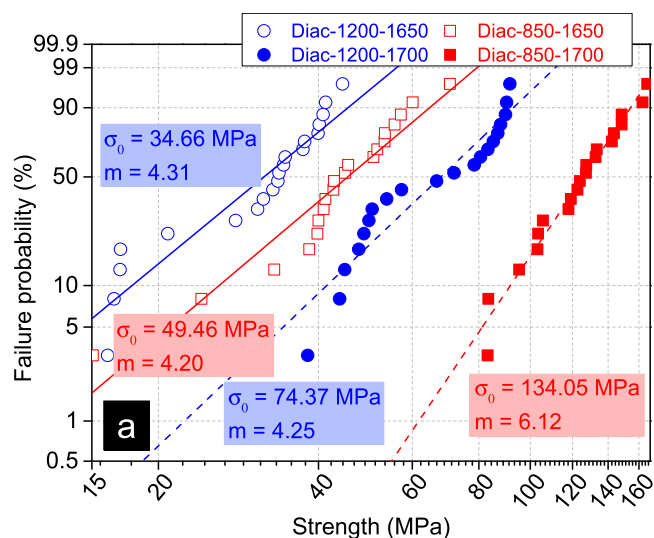
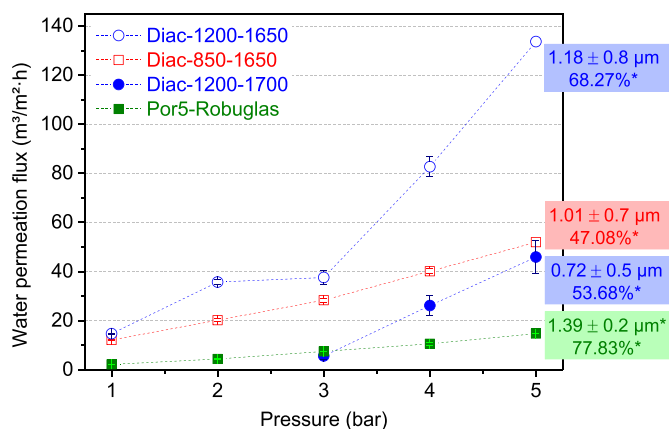


Fig. 6. (a) Weibull failure distribution of flexural strength of selected sintered membranes measured by three-point bending test; (b) flexural strength as a function of open porosity for tested membranes and literature comparison (She and Ohji “▲” [42], Dong et al. “▼” [43], Cao et al. “◆” [25], Hou et al. “◀” [29], and Hua et al. “▶” [44]). (Diac-X-X samples in Fig. 6b followed by different letters were significantly different at  $p < 0.05$  according to Tukey’s test).

850-1XXX specimens and all samples sintered at 1600 °C could not be tested due to their high brittle response, which made the preparation (cutting) of these samples impossible. The samples sintered at 1700 °C display higher flexural strength, 134 MPa for Diac-850-1700 and 74.37 MPa for Diac-1200-1700. Meanwhile, Diac-850-1650 and Diac-1200-1650 present  $\sigma_0$  values equal to 49.46 MPa and 34.66 MPa, respectively. However, the  $m$  value is in the range of 4 for all studied membranes except for Diac-850-1700 ( $m = 6$ ). This distinct value can be correlated to the inferior open porosity compared to the other specimens, as shown in Fig. 6b. Furthermore, Fig. 6b also shows that the obtained flexural strength–porosity pairs in this work are comparable to values reported in the literature (taking into consideration 3 point bending tests of porous mullite). Tukey’s test ( $p < 0.05$ ) shows that the samples sintered at 1700 °C are statistically different (in terms of flexural strength) from each other and from the samples sintered at 1650 °C. However, Diac-850-1650 and Diac-1200-1650 samples do not display any significant difference according to Tukey’s multiple comparison test despite the expressive difference with regard to the open porosity. All the presented data denote a negative linear relationship between flexural strength and porosity, as expected.



**Fig. 7.** Water permeation flux ( $\text{m}^3/\text{m}^2\cdot\text{h}$ ) as a function of the applied pressure (bar) for selected membranes in a dead-end configuration (the values inside the colored boxes represent the average pore size (top) and the open porosity (bottom). Values signed with “\*” were obtained from Hg-porosimetry; values without markers were determined by image analysis from SEM pictures of the top surface).

### 3.5. Membrane performance and transport properties

The water permeation flux according to the applied pressure for some selected membranes is shown in Fig. 7. The composition Diac-850-1700 is not displayed here due to the poor permeability observed during the tests. For comparison purposes, a commercial borosilicate glass membrane (Por5 from Robuglas) with a symmetric pore structure was also studied. This membrane has an average pore diameter of  $1.39\ \mu\text{m}$  and open porosity about 78% as determined by Hg-porosimetry (Fig.S. 4). Despite the larger average pore size and its elevated open porosity, the commercial membrane presents the lowest water permeation flux among the tested membranes. Nevertheless, it is noticed a 6.7 times increase in flux when raising the pressure from 1 to 5 bar, resulting on fluxes of  $2.2\ \text{m}^3/\text{m}^2\cdot\text{h}$  and  $14.7\ \text{m}^3/\text{m}^2\cdot\text{h}$ , respectively. The prepared asymmetric mullite membranes show a superior flux increase with the applied pressures. Diac-1200-1650 exhibits the best outcome, in which the water flux increases from  $14.7\ \text{m}^3/\text{m}^2\cdot\text{h}$  up to  $133.6\ \text{m}^3/\text{m}^2\cdot\text{h}$  ( $\sim 9.1$  times increment), just by changing the pressure from 1 bar to 5 bar. Samples Diac-850-1650 and Diac-1200-1700 differ in terms of water flux at pressures below 5 bar but show quite similar values at 5 bar,  $52.0\ \text{m}^3/\text{m}^2\cdot\text{h}$  and  $45.9\ \text{m}^3/\text{m}^2\cdot\text{h}$ , respectively.

Table 3 summarizes the transport properties of the studied membranes based on the pure water permeation test (Fig S. 5 with the linear fittings and the considered equations are detailed in the supplementary material). The asymmetric membranes exhibited a similar thickness ( $\delta_m$ ) in the range of 6–8  $\mu\text{m}$ , while the symmetric commercial membrane presents the thickness in the millimeter range ( $\sim 1\ \text{mm}$ ). Despite the slight inferior water flux output and permeance presented by Diac-1200-1700 compared to Diac-850-1650, the membrane resistance and the intrinsic permeability of Diac-1200-1700 are superior due to the slight thinner skin-layer ( $\delta_m$ ). However, due to the impossibility of

**Table 3**

Membrane thickness ( $\delta_m$ ) and transport properties in terms of permeance ( $k_w$ ), clean membrane resistance ( $R_m$ ), and intrinsic permeability ( $k_{v,intr}$ ) of the tested asymmetric and symmetric ceramic membranes.

Sample	$\delta_m$ (m)	$k_w$ ( $\text{m}^3/\text{m}^2\cdot\text{h}\cdot\text{bar}$ )	$R_m$ ( $\text{m}^{-1}$ )	$k_{v,intr}$ ( $\text{m}^2$ )
Diac-1200-1650	$6.11 \times 10^{-6}$	$21.78 \pm 2.62$	$1.86 \times 10^{10}$	$3.29 \times 10^{-16}$
Diac-1200-1700	$7.66 \times 10^{-6}$	$7.02 \pm 1.89$	$5.76 \times 10^{10}$	$1.33 \times 10^{-16}$
Diac-850-1650	$6.86 \times 10^{-6}$	$10.14 \pm 0.21$	$3.99 \times 10^{10}$	$1.72 \times 10^{-16}$
Por5-Robuglas	$1.00 \times 10^{-3}$	$2.72 \pm 0.12$	$1.49 \times 10^{11}$	$6.72 \times 10^{-15}$

acquiring more data points regarding the water flux of Diac-1200-1700, the calculated transport properties should be carefully considered. As one may expect, the symmetric thick Por5 membrane shows lowest permeance ( $2.72 \pm 0.12\ \text{m}^3/\text{m}^2\cdot\text{h}\cdot\text{bar}$ ) and inferior permeability ( $6.72 \times 10^{-15}\ \text{m}^2$ ). Diac-1200-1650 displays the highest permeance ( $k_w = 21.78 \pm 2.62\ \text{m}^3/\text{m}^2\cdot\text{h}\cdot\text{bar}$ ) and intrinsic permeability ( $k_{v,intr} = 3.29 \times 10^{-16}\ \text{m}^2$ ), hence the lowest membrane resistance ( $R_m = 1.86 \times 10^{10}\ \text{m}^{-1}$ ).

## 4. Discussion

This work revealed that the stoichiometric combination of polysiloxane and aluminum diacetate is feasible to synthesize high-purity mullite ( $3\text{Al}_2\text{O}_3\cdot 2\text{SiO}_2$ ) crystal phase at relatively low temperature ( $1200\ ^\circ\text{C}$ ) and short holding time (3 h). Even though the SEM images from the powder (Fig. 2) show some extent of agglomeration according to the alumina precursor and calcining temperature, the mullitization is not hindered for the sample Diac-1200. This is possible due to the high reactivity of the precursors during thermooxidative treatment. The thermo-oxidational degradation of polysiloxane in oxygen-containing atmospheres leads to the development of highly reactive amorphous  $\text{SiO}_2$  [22,23,45]. Regarding the aluminum diacetate, the literature reports that its thermal oxidation results in reactive amorphous alumina at low temperature ( $\sim 450\ ^\circ\text{C}$ ), which is converted into  $\gamma\text{-Al}_2\text{O}_3$  at around  $860\ ^\circ\text{C}$ , followed by a phase transformation to  $\alpha\text{-Al}_2\text{O}_3$  at  $1150\ ^\circ\text{C}$  [31]. Despite the fact that only Diac-1200 resulted in mullite phase during the calcination of the powders, all the prepared membranes originate mullite phase above 99% after sintering (Table 2). This is quite expected given the applied temperatures; however, it is important to stress that high-purity mullite was produced under reasonably shorter holding time (2 h) compared to traditional methods [46,47].

The membrane morphology in the phase-inversion process is dictated primarily by the composition of both the slurry and the precipitation bath. Since this study did not focus on evaluating different non-solvents, the morphology has to be explained in terms of slurry composition. In this regard, the main difference among the samples is the particle size of the mullite-based powder. It is well known that the particle has a direct influence on the rheology of the system [13,17]. Generally, when comparing similar ceramic slurries compositions, the particle size is found to be inversely proportional to slurry viscosity (see Fig. 2 and Fig.S. 3). However, the formation of finger-like voids (observed in the Alu-850 and Diac-1200 samples) is favored by reducing the viscosity of the system, intensifying the viscous fingering phenomena [48,49]. Diac-850 specimen only shows the skin-layer followed by the sponge-layer. This indicates that the viscosity threshold at which the finger-like structure can be completely suppressed was reached for the referred composition.

The average pore size distribution and open porosity displayed in Fig. 5 clearly reflect the particle size and distribution of their respective precursor powders (Fig. 2). As evident from these figures, the narrower the particle size distribution the narrower is the resultant pore size distribution. The same interpretation can be transferred to the average values of the particle and pore size [50]. With respect to the open porosity, the same trend can be inferred. Moreover, the Diac-850-1XXX samples possibly have an additional feature that led to a more pronounced reduction of open porosity, which is the implied higher reactivity compared to the other mullite-based powders. This hypothesis may be sustained by the XRD data in Fig. 3, which can indicate a latent potential of the amorphous Diac-850 powder for reacting and/or sintering.

The evaluation of the mechanical properties of brittle materials normally requires plenty of caution, especially when dealing with porous ceramics. Therefore, Weibull analysis consists of a suitable method to analyze the mechanical performance of such components [51]. The degradation of the mechanical strength due to the presence of

pores/porosity is well defined in the literature. Hence, pores are characterized as macrodefects in the ceramic structure. Nevertheless, it is worth mentioning that porosity has little effect on the bending strength if porosity is over 30% [52]. This is probably the main reason for the higher flexural strength exhibited by Diac-850-1700 ( $\sigma_0$ : 134 MPa; Open porosity: 33%). Another factor that perhaps impacted on this result could be related to Diac-850 morphology, in which the exclusive presence of sponge-layer configuration results in a more concise macrostructure than the finger-like layer [48,53].

As previously mentioned, Fig. 7 illustrates the water permeation performance for selected asymmetric mullite membranes and a commercial symmetric borosilicate membrane (Por5). Taking into account the pore size and porosity displayed, it is possible to infer that both parameters have a direct influence on permeation flux. Nonetheless, this assumption is mostly valid if Por5 is not considered. When Por5 is compared to the prepared membranes, the aforementioned assumption does not sustain itself. Therefore, the asymmetric morphology is playing a major role in membrane performance, in which the porous support minimizes mass transport limitations [54–56]. Furthermore, the determined transport properties corroborates the superior performance of the asymmetric membranes, especially Diac-1200-1650, in which the clean membrane resistance ( $R_m$ ) is almost one order of magnitude below the usual range given in literature for microfiltration membranes ( $1 \times 10^{11} - 1 \times 10^{12} \text{ m}^{-1}$ ) [57,58].

## 5. Conclusions

Asymmetric mullite membranes in the microfiltration range were successfully prepared by phase-inversion tape casting. The mullite powder was produced by using polymethylsiloxane as silica precursor and aluminum diacetate as alumina source. Almost complete mullitization could be achieved after 3 h at 1200 °C from these precursors. There is a great potential in preparing high-purity mullite using polysiloxanes in combination with aluminum diacetate. The membrane morphology varied due to slurry viscosity, which depends on the ceramic particle size in this case. The increase in viscosity by using smaller mullite-based powder (Diac-850) suppressed the formation of finger-like layer. Nevertheless, samples prepared with Diac-1200 and Alu-850 exhibited a skin-layer followed by a porous support composed by a mix of finger-like and sponge-like structures. Moreover, all membranes presented a pore size range on the skin-layer in the microfiltration range (0.4–2  $\mu\text{m}$ ). However, due to mechanical constraints and porosity some membranes were not suitable to be further characterized. Among the tested samples the Diac-1200-1650 specimen seems to be prospective to be applied in membrane technology, given its outstanding water flux and transport properties.

## Acknowledgments

This study was financed in part by the Brazilian Coordination for the Improvement of Higher Education Personnel (CAPES) through the Brazilian-German Collaborative Research Initiative on Manufacturing (BRAGECRIM) Program. The German Research Foundation (DFG) as well as the Brazilian National Council for Scientific and Technological Development (CNPq) are also gratefully acknowledged. The authors thank Laura Luhede and Alexander Schulz at the Leibniz-Institut für Werkstofforientierte Technologien for helping with the measurement of the particle size and slurry viscosity, respectively. Wenhui Zhong is also acknowledged by performing water permeation tests.

## Appendix A. Supplementary data

Supplementary data to this article can be found online at <https://doi.org/10.1016/j.memsci.2019.03.047>.

## References

- [1] S. Benfer, P. Árki, G. Tomandl, Ceramic membranes for filtration applications — preparation and characterization, *Adv. Eng. Mater.* 6 (2004) 495–500, <https://doi.org/10.1002/adem.200400577>.
- [2] S. Luque, D. Gómez, J.R. Álvarez, Industrial applications of porous ceramic membranes (pressure-driven processes), *Membr. Sci. Technol.* 13 (2008) 177–216, [https://doi.org/10.1016/S0927-5193\(07\)13006-0](https://doi.org/10.1016/S0927-5193(07)13006-0).
- [3] D. da Silva Biron, V. dos Santos, M. Zeni, Ceramic Membranes Applied in Separation Processes, (2018), <https://doi.org/10.1007/978-3-319-58604-5>.
- [4] H. Fang, C. Ren, Y. Liu, D. Lu, L. Winnubst, C. Chen, Phase-inversion tape casting and synchrotron-radiation computed tomography analysis of porous alumina, *J. Eur. Ceram. Soc.* 33 (2013) 2049–2051 <https://doi.org/10.1016/j.jeurceramsoc.2013.02.032>.
- [5] W. He, H. Huang, J. fen Gao, L. Winnubst, C. sheng Chen, Phase-inversion tape casting and oxygen permeation properties of supported ceramic membranes, *J. Membr. Sci.* 452 (2014) 294–299, <https://doi.org/10.1016/j.memsci.2013.09.063>.
- [6] R.H. Yuan, W. He, Y. Zhang, J.F. Gao, C.S. Chen, Preparation and characterization of supported planar  $\text{Zr}_{0.84}\text{Y}_{0.16}\text{O}_{1.92}\text{-La}_{0.8}\text{Sr}_{0.2}\text{Ce}_{0.5}\text{Fe}_{0.5}\text{O}_{3-\delta}$  composite membrane, *J. Membr. Sci.* 499 (2016) 335–342, <https://doi.org/10.1016/j.memsci.2015.10.066>.
- [7] J. Gu, C. Ren, X. Zong, C. Chen, L. Winnubst, Preparation of alumina membranes comprising a thin separation layer and a support with straight open pores for water desalination, *Ceram. Int.* 42 (2016) 12427–12434 <https://doi.org/10.1016/j.ceramint.2016.04.183>.
- [8] J. Gao, X. Meng, T. Luo, H. Wu, Z. Zhan, Symmetrical solid oxide fuel cells fabricated by phase inversion tape casting with impregnated SrFe 0.75 Mo 0.25 O 3- $\delta$  (SFMO) electrodes, *Int. J. Hydrogen Energy* (2017) 3–7, <https://doi.org/10.1016/j.ijhydene.2017.03.205>.
- [9] Y. Meng, W. He, X. Li, J. Gao, Z. Zhan, J. Yi, C. Chen, H.J.M. Bouwmeester, Asymmetric La 0.6 Sr 0.4 Co 0.2 Fe 0.8 O 3- $\delta$  membrane with reduced concentration polarization prepared by phase-inversion tape casting and warm pressing, *J. Membr. Sci.* 533 (2017) 11–18, <https://doi.org/10.1016/j.memsci.2017.03.025>.
- [10] R.K. Nishihora, P.L. Rachadel, M.G.N. Quadri, D. Hotza, Manufacturing porous ceramic materials by tape casting-A review, *J. Eur. Ceram. Soc.* 38 (2018) 988–1001, <https://doi.org/10.1016/j.jeurceramsoc.2017.11.047>.
- [11] E. Drioli, L. Giorno, *Comprehensive Membrane Science and Engineering*, Elsevier, 2010.
- [12] N. Yang, X. Tan, Z. Ma, A phase inversion/sintering process to fabricate nickel/yttria-stabilized zirconia hollow fibers as the anode support for micro-tubular solid oxide fuel cells, *J. Power Sources* 183 (2008) 14–19 <https://doi.org/10.1016/j.jpowsour.2008.05.006>.
- [13] S.K. Hubadillah, Z. Harun, M.H.D. Othman, A.F. Ismail, W.N.W. Salleh, H. Basri, M.Z. Yunos, P. Gani, Preparation and characterization of low cost porous ceramic membrane support from kaolin using phase inversion/sintering technique for gas separation: effect of kaolin content and non-solvent coagulant bath, *Chem. Eng. Res. Des.* 112 (2016) 24–35, <https://doi.org/10.1016/j.cherd.2016.06.007>.
- [14] D.D. Athayde, D.F. Souza, A.M.A. Silva, D. Vasconcelos, E.H.M. Nunes, J.C. Diniz da Costa, W.L. Vasconcelos, Review of perovskite ceramic synthesis and membrane preparation methods, *Ceram. Int.* 42 (2016) 6555–6571 <https://doi.org/10.1016/j.ceramint.2016.01.130>.
- [15] N. Hilal, A.F. Ismail, C. Wright, *Membrane Fabrication*, CRC Press, 2015.
- [16] H.P. Hsieh, *Inorganic Membranes for Separation and Reaction*, Elsevier Science, 1996.
- [17] S.K. Hubadillah, Z. Harun, M.H.D. Othman, A.F. Ismail, P. Gani, Effect of kaolin particle size and loading on the characteristics of kaolin ceramic support prepared via phase inversion technique, *J. Asian Ceram. Soc.* 4 (2016) 164–177, <https://doi.org/10.1016/j.jascer.2016.02.002>.
- [18] G.R. Guillen, Y. Pan, M. Li, E.M.V. Hoek, Preparation and characterization of membranes formed by nonsolvent induced phase separation: a review, *Ind. Eng. Chem. Res.* 50 (2011) 3798–3817, <https://doi.org/10.1021/ie101928r>.
- [19] R.F. Davis, J.A. Pask, Mullite, *Refract. Glas. Glas. Ceram. - High Temp. Oxides*, 1971, pp. 37–76, <https://doi.org/10.1016/B978-0-12-053304-6.50011-4> Part IV.
- [20] H. Schneider, J. Schreuer, B. Hildmann, Structure and properties of mullite-A review, *J. Eur. Ceram. Soc.* 28 (2008) 329–344, <https://doi.org/10.1016/j.jeurceramsoc.2007.03.017>.
- [21] M.F. Serra, M.S. Conconi, M.R. Gauna, G. Suárez, E.F. Aglietti, N.M. Rendtorff, Mullite (3Al<sub>2</sub>O<sub>3</sub>·2SiO<sub>2</sub>) ceramics obtained by reaction sintering of rice husk ash and alumina, phase evolution, sintering and microstructure, *J. Asian Ceram. Soc.* 4 (2016) 61–67, <https://doi.org/10.1016/j.jascer.2015.11.003>.
- [22] D. Suttor, H.-J. Kleebe, G. Ziegler, Formation of mullite from filled siloxanes, *J. Am. Ceram. Soc.* 80 (1997) 2541–2548, <https://doi.org/10.1111/j.1151-2916.1997.tb03156.x>.
- [23] E. Bernardo, P. Colombo, E. Pippel, J. Woltersdorf, Novel mullite synthesis based on alumina nanoparticles and a preceramic polymer, *J. Am. Ceram. Soc.* 89 (2006) 1577–1583, <https://doi.org/10.1111/j.1551-2916.2006.00963.x>.
- [24] L. Li, M. Chen, Y. Dong, X. Dong, S. Cerneaux, S. Hampshire, J. Cao, L. Zhu, Z. Zhu, J. Liu, A low-cost alumina-mullite composite hollow fiber ceramic membrane fabricated via phase-inversion and sintering method, *J. Eur. Ceram. Soc.* 36 (2015) 2057–2066, <https://doi.org/10.1016/j.jeurceramsoc.2016.02.020>.
- [25] J. Cao, X. Dong, L. Li, Y. Dong, S. Hampshire, Recycling of waste fly ash for production of porous mullite ceramic membrane supports with increased porosity, *J. Eur. Ceram. Soc.* 34 (2014) 3181–3194, <https://doi.org/10.1016/j.jeurceramsoc.2014.04.011>.
- [26] M. Chen, L. Zhu, Y. Dong, L. Li, J. Liu, Waste-to-Resource strategy to fabricate

- highly porous whisker-structured mullite ceramic membrane for simulated oil-in-water emulsion wastewater treatment, *ACS Sustain. Chem. Eng.* 4 (2016) 2098–2106, <https://doi.org/10.1021/acssuschemeng.5b01519>.
- [27] Z. Cuo, H. Liu, F. Zhao, W. Li, S. Peng, Y. Chen, Highly porous fibrous mullite ceramic membrane with interconnected pores for high performance dust removal, *Ceram. Int.* 44 (2018) 11778–11782, <https://doi.org/10.1016/j.ceramint.2018.03.259>.
- [28] S.K. Hubadillah, M.H.D. Othman, T. Matsuura, A.F. Ismail, M.A. Rahman, Z. Harun, J. Jaafar, M. Nomura, Fabrications and applications of low cost ceramic membrane from kaolin: a comprehensive review, *Ceram. Int.* 44 (2018) 4538–4560, <https://doi.org/10.1016/j.ceramint.2017.12.215>.
- [29] Z. Hou, B. Cui, L. Liu, Q. Liu, Effect of the different additives on the fabrication of porous kaolin-based mullite ceramics, *Ceram. Int.* 42 (2016) 17254–17258, <https://doi.org/10.1016/j.ceramint.2016.08.020>.
- [30] J. Ma, F. Ye, B. Zhang, Y. Jin, C. Yang, J. Ding, H. Zhang, Q. Liu, Low-temperature synthesis of highly porous whisker-structured mullite ceramic from kaolin, *Ceram. Int.* 44 (2018) 13320–13327, <https://doi.org/10.1016/j.ceramint.2018.04.163>.
- [31] R.R. Menezes, E. Fagury-Neto, M.C. Fernandes, P.M. Souto, R.H.G. a. Kiminami, Obtenção de mullita porosa a partir da sílica da casca de arroz e do acetato de alumínio, *Cerâmica* 54 (2008) 245–252, <https://doi.org/10.1590/S0366-69132008000200015>.
- [32] C.A. Schneider, W.S. Rasband, K.W. Eliceiri, NIH Image to ImageJ: 25 years of image analysis, *Nat. Methods* 9 (2012) 671–675, <https://doi.org/10.1038/nmeth.2089>.
- [33] L. Lutterotti, M. Bortolotti, G. Ischia, I. Lonardelli, H.R. Wenk, Rietveld texture analysis from diffraction images, *Z. Kristallogr. Suppl.* 2007 (2007) 125–130, <https://doi.org/10.1524/zksu.2007.2007.suppl.26.125>.
- [34] L. Lutterotti, MAUD - Materials Analysis Using Diffraction, (2019) <http://maud.radiographema.eu/>.
- [35] S. Gražulis, A. Daškevič, A. Merkys, D. Chateigner, L. Lutterotti, M. Quirós, N.R. Serebryanaya, P. Moeck, R.T. Downs, A. LeBail, Crystallography Open Database (COD): an open-access collection of crystal structures and platform for world-wide collaboration, *Nucleic Acids Res.* 40 (2012) D420–D427, <https://doi.org/10.1093/nar/gkr900>.
- [36] COD, Crystallography Open Database, (2019) <http://www.crystallography.net/cod/index.php>.
- [37] D.E. 843-1, *Advanced Technical Ceramics - Mechanical Properties of Monolithic Ceramics at Room Temperature - Part I: Determination of Flexural Strength*, Beuth, 2006.
- [38] F.H. Liu, Y.S. Liao, Fabrication of inner complex ceramic parts by selective laser sintering, *J. Eur. Ceram. Soc.* 30 (2010) 3283–3289, <https://doi.org/10.1016/j.jeurceramsoc.2010.08.001>.
- [39] F. Dogan, J. Feng, L.G. Ferguson, Method for Sintering Ceramic tapes, (2002) 6447712 <http://www.freepatentsonline.com/6447712.html>.
- [40] Z. Nakagawa, T. Aosaki, N. Enomoto, Crystallization process of amorphous aluminas to  $\alpha$ -alumina, *Mater. Sci. Eng. Serv. Soc.* (1998) 52–55, <https://doi.org/10.1016/B978-044482793-7/50015-1>.
- [41] I.G. Polyakova, 4. The main silica phases and some of their properties, in: J.W.P. Schmelzer (Ed.), *Glas. Sel. Prop. Cryst. De Gruyter*, Berlin, Boston, 2014, pp. 197–268, <https://doi.org/10.1515/9783110298581.197>.
- [42] J.H. She, T. Ohji, Porous mullite ceramics with high strength, *J. Mater. Sci. Lett.* 21 (2002) 1833–1834, <https://doi.org/10.1023/A:1021576104859>.
- [43] Y. Dong, J. er Zhou, B. Lin, Y. Wang, S. Wang, L. Miao, Y. Lang, X. Liu, G. Meng, Reaction-sintered porous mineral-based mullite ceramic membrane supports made from recycled materials, *J. Hazard Mater.* 172 (2009) 180–186, <https://doi.org/10.1016/j.jhazmat.2009.06.148>.
- [44] K. Hua, A. Shui, L. Xu, K. Zhao, Q. Zhou, X. Xi, Fabrication and characterization of anorthite-mullite-corundum porous ceramics from construction waste, *Ceram. Int.* 42 (2016) 6080–6087, <https://doi.org/10.1016/j.ceramint.2015.12.165>.
- [45] B.V. Manoj Kumar, Y.-W. Kim, Processing of polysiloxane-derived porous ceramics: a review, *Sci. Technol. Adv. Mater.* 11 (2010) 44303, <https://doi.org/10.1088/1468-6996/11/4/044303>.
- [46] M.D. Sacks, J.A. Pask, Sintering of mullite-containing materials: II, effect of agglomeration, *J. Am. Ceram. Soc.* 65 (1982) 70–77, <https://doi.org/10.1111/j.1151-2916.1982.tb10360.x>.
- [47] L. Montanaro, J.M. Tulliani, C. Perrot, A. Negro, Sintering of industrial mullites, *J. Eur. Ceram. Soc.* 17 (1997) 1715–1723, [https://doi.org/10.1016/S0955-2219\(97\)00043-5](https://doi.org/10.1016/S0955-2219(97)00043-5).
- [48] B.F.K. Kingsbury, K. Li, A morphological study of ceramic hollow fibre membranes, *J. Membr. Sci.* 328 (2009) 134–140, <https://doi.org/10.1016/j.memsci.2008.11.050>.
- [49] B. Wang, Z. Lai, Finger-like voids induced by viscous fingering during phase inversion of alumina/PES/NMP suspensions, *J. Membr. Sci.* 405–406 (2012) 275–283, <https://doi.org/10.1016/j.memsci.2012.03.020>.
- [50] N. Das, H.S. Maiti, Effect of size distribution of the starting powder on the pore size and its distribution of tape cast alumina microporous membranes, *J. Eur. Ceram. Soc.* 19 (1999) 341–345 [https://doi.org/10.1016/S0955-2219\(98\)00205-2](https://doi.org/10.1016/S0955-2219(98)00205-2).
- [51] R. Danzer, P. Supancic, J. Pascual, T. Lube, Fracture statistics of ceramics - Weibull statistics and deviations from Weibull statistics, *Eng. Fract. Mech.* 74 (2007) 2919–2932, <https://doi.org/10.1016/j.engfracmech.2006.05.028>.
- [52] Q. Chang, Y. Yang, X. Zhang, Y. Wang, J. Zhou, X. Wang, S. Cerneaux, L. Zhu, Y. Dong, Effect of particle size distribution of raw powders on pore size distribution and bending strength of Al<sub>2</sub>O<sub>3</sub> microfiltration membrane supports, *J. Eur. Ceram. Soc.* 34 (2014) 3819–3825 <https://doi.org/10.1016/j.jeurceramsoc.2014.06.001>.
- [53] Z. Wu, B. Wang, K. Li, A novel dual-layer ceramic hollow fibre membrane reactor for methane conversion, *J. Membr. Sci.* 352 (2010) 63–70, <https://doi.org/10.1016/j.memsci.2010.01.062>.
- [54] M. Kukizaki, M. Goto, Preparation and characterization of a new asymmetric type of Shirasu porous glass (SPG) membrane used for membrane emulsification, *J. Membr. Sci.* 299 (2007) 190–199, <https://doi.org/10.1016/j.memsci.2007.04.040>.
- [55] X. Chang, C. Zhang, Y. He, X. Dong, W. Jing, N. Xu, A comparative study of the performance of symmetric and asymmetric mixed-conducting membranes, *Chin. J. Chem. Eng.* 17 (2009) 562–570, [https://doi.org/10.1016/S1004-9541\(08\)60245-1](https://doi.org/10.1016/S1004-9541(08)60245-1).
- [56] L. Chen, L. Liu, J. Xue, L. Zhuang, H. Wang, Asymmetric membrane structure: an efficient approach to enhance hydrogen separation performance, *Separ. Purif. Technol.* 207 (2018) 363–369, <https://doi.org/10.1016/j.seppur.2018.06.066>.
- [57] M. Li, Y. Zhao, S. Zhou, W. Xing, F.S. Wong, Resistance analysis for ceramic membrane microfiltration of raw soy sauce, *J. Membr. Sci.* 299 (2007) 122–129, <https://doi.org/10.1016/j.memsci.2007.04.033>.
- [58] M.M. Benjamin, D.F. Lawler, *Water Quality Engineering: Physical/Chemical Treatment Processes*, Wiley, 2013.